The type II transmembrane serine protease matriptase cleaves the amyloid precursor protein and reduces its processing to β-amyloid peptide

Received for publication, April 25, 2017, and in revised form, October 16, 2017 Published, Papers in Press, October 20, 2017, DOI 10.1074/jbc.M117.792911

Erwan Lanchec[‡], Antoine Désilets[‡], François Béliveau[‡], Anthony Flamier[§], Shaimaa Mahmoud[¶], Gilbert Bernier[§‖], Denis Gris[¶], Richard Leduc[‡1], and Christine Lavoie[‡2]

From the [‡]Department of Pharmacology-Physiology, Faculty of Medicine and Health Sciences, Université de Sherbrooke, Sherbrooke, Quebec J1H5N4, Canada, [§]Stem Cell and Developmental Biology Laboratory, Hôpital Maisonneuve-Rosemont, 5415 Boulevard de l'Assomption, Montréal, Quebec H1T 2M4, Canada, [¶]Department of Pediatrics, Faculty of Medicine and Health Sciences, Université de Sherbrooke, Sherbrooke, Quebec J1H5N4, Canada, and [‖]Department of Neurosciences, Université de Montréal, Montréal, Quebec H3C 3J7, Canada

Edited by Paul E. Fraser

Recent studies have reported that many proteases, besides the canonical α-, β-, and γ-secretases, cleave the amyloid precursor protein (APP) and modulate β-amyloid (Aβ) peptide production. Moreover, specific APP isoforms contain Kunitz protease-inhibitory domains, which regulate the proteolytic activity of serine proteases. This prompted us to investigate the role of matriptase, a member of the type II transmembrane serine protease family, in APP processing. Using quantitative RT-PCR, we detected matriptase mRNA in several regions of the human brain with an enrichment in neurons. RNA sequencing data of human dorsolateral prefrontal cortex revealed relatively high levels of matriptase RNA in young individuals, whereas lower levels were detected in older individuals. We further demonstrate that matriptase and APP directly interact with each other and that matriptase cleaves APP at a specific arginine residue (Arg-102) both *in vitro* and in cells. Site-directed (Arg-to-Ala) mutagenesis of this cleavage site abolished matriptase-mediated APP processing. Moreover, we observed that a soluble, shed matriptase form cleaves endogenous APP in SH-SY5Y cells and that this cleavage significantly reduces APP processing to Aβ40. In summary, this study identifies matriptase as an APP-cleaving enzyme, an activity that could have important consequences for the abundance of Aβ and in Alzheimer's disease pathology.

Alzheimer's disease (AD)[3] is characterized by a progressive degeneration of neurons, which results in cognitive disturbances. One of the main hallmarks found in the brains of AD patients is the presence of amyloid plaques, mainly composed of the β-amyloid (Aβ) peptide generated through processing of the amyloid precursor protein (APP) (1). There are different isoforms of APP; the major ones in the brain are APP770, APP751, and APP695 (2). These isoforms differ by the presence of a 19-amino-acid OX-2 domain, which has similarities with the OX-2 antigen of lymphoid cells, and of a 56-amino-acid Kunitz protease-inhibitory (KPI) domain, which is known for its ability to inhibit serine proteases (2–4). The longest isoform, APP770, contains both KPI and OX-2 domains, whereas APP751 only contains the KPI domain. In contrast, the shortest and neuron-specific isoform, APP695, lacks both KPI and OX-2 domains. In AD, there is an increase of APP770 and APP751 mRNAs but no increase of APP695 mRNA (5). It has been suggested that this increased expression of APP mRNA containing the KPI domain could play an important role in protecting the protein from proteolysis (6).

The three APP isoforms undergo proteolytic cleavage by several compartmentalized secretases (1). In the amyloidogenic pathway, APP is initially processed by β-secretase to produce a soluble secreted form of APP (sAPPβ) and a C-terminal fragment (β-CTF). The subsequent cleavage of β-CTF by γ-secretase yields the Aβ peptide and the amyloid precursor protein intracellular domain. In the non-amyloidogenic pathway, APP is first cleaved by α-secretase within the Aβ sequence to generate the soluble secreted sAPPα fragment and the membrane-tethered α-CTF. This is followed by γ-secretase cleavage of α-CTF, resulting in release of the P3 peptide and amyloid precursor protein intracellular domain. Many other enzymes are capable of proteolytically processing APP; for example, β2-secretase (also called θ-secretase) cleaves APP within the Aβ peptide, thus preventing Aβ peptide production (7). Also, serine proteases such as high-temperature requirement A (htrA) 1 and 2, contribute to APP and Aβ degradation (8, 9).

This work was supported by Pfizer-Fonds de Recherche du Québec-Santé Innovation Funds for Alzheimer Disease and Related Disorders. The authors declare that they have no conflicts of interest with the contents of this article.

This article contains supplemental Methods, Figs. S1–S6, and Tables S1 and S2.

[1] To whom correspondence may be addressed. Tel.: 819-821-8000 (ext. 75413); E-mail: Richard.Leduc@USherbrooke.ca.

[2] To whom correspondence may be addressed. Tel.: 819-821-8000 (ext. 72732); E-mail: Christine.L.Lavoie@USherbrooke.ca.

[3] The abbreviations used are: AD, Alzheimer's disease; APP, amyloid precursor protein; Aβ, β-amyloid; KPI, Kunitz protease-inhibitory; RNA-seq, RNA sequencing; sAPP, soluble secreted form of APP; CTF, C-terminal fragment; TTSP, type II transmembrane serine protease; ST14, suppression of tumorigenicity-14; HAI-1 and HAI-2, hepatocyte growth factor activator inhibitor types 1 and 2; qPCR, quantitative PCR; hiPSCs, human induced pluripotent stem cells; DLPC, dorsolateral prefrontal cortex; N-term, extracellular region; C-term, cytoplasmic region; APLP, amyloid precursor-like protein.

Therefore, APP-processing proteases are the subject of an increasing number of studies related to AD.

Within the extracellular space in vertebrates, several proteases act as essential modulators of development and tissue remodeling (10). One of these, matriptase, is a member of the type II transmembrane serine protease (TTSP) family that is encoded by the suppression of tumorigenicity-14 (*ST14*) gene (11). Matriptase is mostly expressed in epithelial cells (12) and involved in development and maintenance of epithelial barrier integrity such as in the skin and gut (11). This protease is a cell-surface glycoprotein that undergoes catalytic autoactivation and is released from the cell surface as a soluble, shed form to the pericellular environment (13). Indeed, matriptase had initially been identified in the culture medium of breast cancer cells and detected in human milk (12, 14, 15). This shed form of matriptase can thus interact with proteins located at the cell surface or in the extracellular matrix. Numerous matriptase substrates have been identified, including hepatocyte growth factor (16), prostasin (17), urokinase-type plasminogen activator (18), protease-activated receptor 2 (18), and epithelial cell adhesion molecule (19). The serine protease catalytic activity of matriptase is physiologically controlled by interaction with hepatocyte growth factor activator inhibitor types 1 and 2 (HAI-1 and HAI-2) through their KPI domain (20). This regulation is essential for proper function of matriptase in adult and embryonic tissues (12, 21).

Although matriptase was originally described as solely expressed in epithelial cells, it was shown that loss of inhibition of matriptase disrupts neural tube closure in mice (21), suggesting that it plays a role in neurogenesis. A recent report also demonstrated that matriptase is expressed in mouse neural progenitor cells and promotes cell migration and neuron differentiation (22), whereas another study revealed the presence of matriptase in human glioblastoma multiform cells where it regulates the neuronal channel ASIC1 (23). Moreover, a member of the TTSP family, matriptase-2, which is almost exclusively expressed in hepatocytes, was shown to alter APP cleavage either indirectly through the activation of the metalloprotease meprin-β, which cleaves APP695 (24), or directly through an interaction with the KPI domain of APP770, which reportedly inhibits matriptase-2 enzymatic activity and protects APP from being processed by this enzyme (25).

Together, these reports led us to investigate whether matriptase is also an APP-cleaving enzyme. Here we show that matriptase is expressed in human brain and neuronal tissues and that the enzyme directly interacts with and cleaves the three APP isoforms at a specific residue in their ectodomains. Furthermore, exogenous addition of matriptase alters Aβ production in neuronal SH-SY5Y cells. These events can have important consequences to the overall processing profile of APP in normal conditions as well as in AD.

Results

Matriptase is expressed in the human brain

To investigate matriptase expression in the human brain, RT-quantitative PCR (qPCR) analysis was performed on postmortem human brain tissues (mean age at death was 73.8 ± 12.2 years) (Fig. 1*A*). mRNA levels of matriptase (*ST14* gene) were measured in human frontal cortex, hippocampus, temporal cortex, and cerebellum tissues. Given that matriptase expression in epithelial cells of intestinal and especially of colon tissue is high (26), the level of matriptase mRNA in the brain region was expressed relative to its expression in colon. Matriptase transcripts were clearly detectable in the frontal cortex, hippocampus, temporal cortex, and cerebellum with no significant difference between the regions tested but at much lower levels than in colon tissue (Fig. 1*A*).

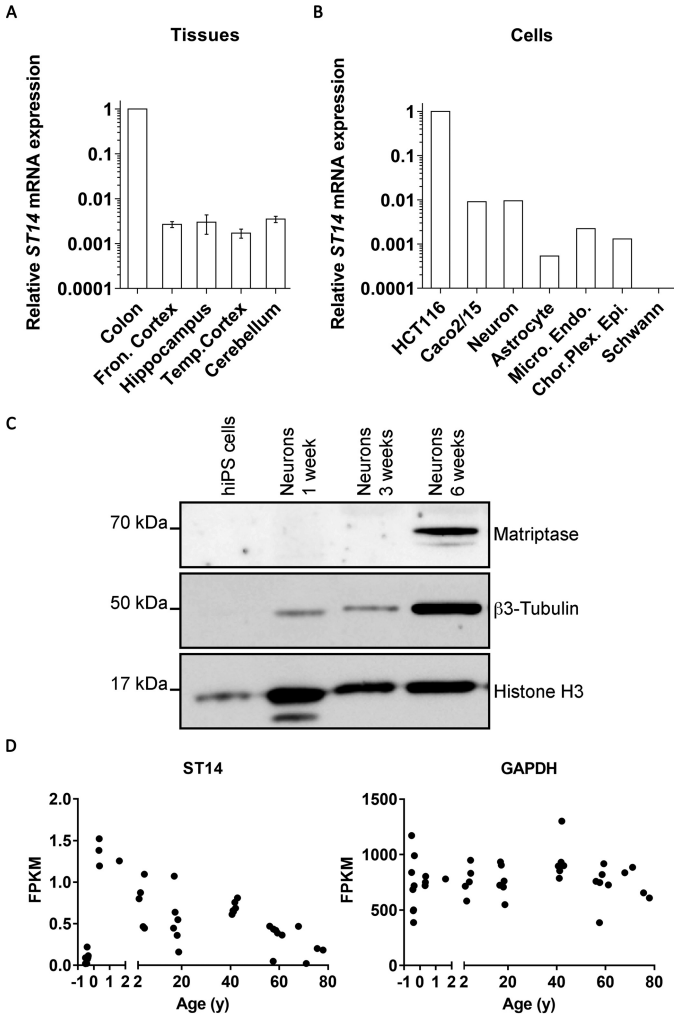

Figure 1. Matriptase (*ST14*) mRNA relative expression in human brains and nervous system cells. *A*, levels of *ST14* mRNA were analyzed in the human frontal (*Fron.*) cortex ($n = 18$), temporal (*Temp.*) cortex ($n = 8$), hippocampus ($n = 5$), and cerebellum ($n = 7$) and expressed relative to that in the human colon tissue ($n = 3$). The difference between the different brain regions was not significant (Student's *t* test, $p > 0.05$). *Error bars* represent means ± S.D. *B*, the levels of *ST14* mRNA were analyzed in human neurons, astrocytes, microvascular endothelial cells (*Micro. Endo.*), choroid plexus epithelial (*Chor. Plex. Epi.*) cells, Schwann cells, and epithelial colorectal adenocarcinoma Caco-2/15 cells and expressed relative to human colon carcinoma HCT116 cells (triplicate analyses were performed on each sample). *C*, expression of matriptase (immunoblot) at different stages of neuronal differentiation (0, 1, 3, and 6 weeks) of hiPSCs. β3-Tubulin was used as neuronal marker, and histone H3 was used as a loading control. *D*, expression levels of *ST14* and *GAPDH* mRNAs across development in the DLPC as measured by fragments per kilobase of exon per million fragments mapped (*FPKM*). Each *dot* represents data from an individual brain. Negative correlation between ages after birth and *ST14* was significant (Spearman's correlation coefficient $r = -0.73$, $p < 0.001$) ($n = 39$).

To ascertain in which cells of the human nervous system matriptase is expressed, RT-qPCR was next performed on total human mRNA from different cell types (Fig. 1*B*). Levels of *ST14* transcripts in these cells were expressed relative to those of human colon carcinoma cells HCT116 (27). Matriptase mRNA was detected in neurons, astrocytes, microvascular endothelial cells, and choroid plexus epithelial cells, whereas no matriptase mRNA was detected in Schwann cells. Interestingly, the mRNA level in neurons was similar to that for human epithelial colorectal adenocarcinoma Caco-2/15 cells. Together, these results reveal matriptase expression in different cell types of the human brain and are in agreement with previous data obtained from mouse brain (22).

Because matriptase was shown to be expressed in mouse differentiating neural progenitor cells (22), we used human induced pluripotent stem cells (hiPSCs) at different stages of neuronal differentiation (0, 1, 3, and 6 weeks) to analyze matriptase protein expression (Fig. 1*C*). From the pluripotent state (hiPSCs) to up to 3 weeks, matriptase is not detected, but a 70-kDa immunoreactive band was detected after 6 weeks of neuronal differentiation. Neuronal differentiation was confirmed by validating the expression of the neuronal markers GABA, vesicular glutamate transporter, NeuN, and β3-tubulin by immunofluorescence (supplemental Fig. S1). The expression of matriptase in differentiated hiPSCs is in line with its detection in mouse neural progenitor cells (22).

On the basis of matriptase expression in mouse brain during development (21, 22), we investigated its ontogeny in the developing human brain. Publicly available RNA sequencing (RNA-seq) data sets of human dorsolateral prefrontal cortex (DLPC) from fetuses, newborns, children, adults, and elderly subjects were retrieved for analysis (28) (Fig. 1*D*). Very low levels of matriptase RNA were detected *in utero*, but much higher levels were found soon after birth. Furthermore, although relatively high levels of matriptase mRNA were found in young brains (age, <20 years), levels were significantly lower in brains of older individuals with a constant decrease over lifetime. Interestingly, these data show a statistically significant negative correlation between age groups (starting after birth) and matriptase RNA levels ($p < 0.001$), whereas no correlation was observed for the housekeeping gene *GAPDH*. Taken together, these results confirm matriptase expression in the human brain and highlight the temporal and spatial modulation of its expression through a lifetime.

Matriptase directly interacts with APP

To investigate whether matriptase can interact with the three major APP isoforms, immunoprecipitations were performed on HEK293 cells transfected with wild-type (WT) matriptase together with GFP-tagged APP770, APP751, or APP695 or GFP (Fig. 2*A*). Matriptase coimmunoprecipitated with GFP-APP770, -APP751, and -APP695 but not with GFP alone (Fig. 2*B*), suggesting that matriptase interacts with all three APP isoforms. Because matriptase associated with GFP-APP695, we conclude that the KPI domain found in isoforms APP770 and APP751 is not required for interaction with the enzyme. GST pulldown assays were next used to verify the *in vitro* interaction between matriptase and the extracellular region of APP695 (GST-APP695 N-term) and/or the cytoplasmic region of APP695 (GST-APP695 C-term) (Fig. 3*A*). ^{35}S-Labeled *in vitro* translated matriptase coprecipitated with GST-APP695 N-term but very weakly with GST-APP695 C-term or GST alone (Fig. 3*B*). Densitometric analysis statistically supports the difference between GST and GST-APP695 N-term and between GST-APP695 C-term and GST-APP695 N-term ($p < 0.05$) (Fig. 3*C*). These results indicate that matriptase interacts directly and predominantly with the N-terminal ectodomain of APP695.

Matriptase cleaves APP

When performing immunoprecipitation with GFP-tagged APP and matriptase, we detected a GFP-APP fragment of 35 kDa in cell lysates (Fig. 2*B*), suggesting cleavage of APP by matriptase. This 35-kDa fragment would correspond to the GFP tag (25 kDa) and a portion of the APP extracellular N terminus (10 kDa). To confirm the role of matriptase in the cleavage of APP and the formation of this APP fragment, HEK293 cells were transfected with GFP-tagged APP770, APP751, and APP695 together with WT matriptase or catalytically inactive matriptase mutant S805A in which the catalytic serine of the active site is replaced with alanine (29) (Fig. 4). Given that the cleavage is expected to occur on the extracellular domain of APP, we also attempted to detect the presence of APP fragments in the culture medium. The GFP-tagged APP fragment of 35 kDa was detected in both cell lysates and conditioned medium of cells transfected with WT matriptase, but not with cells transfected with matriptase S805A, for all three APP isoforms (Fig. 4*A*). In concordance, the levels of GFP-tagged full-length APP (band at 130–150 kDa in cell lysates) or soluble APP (band at 130–150 kDa in medium) were reduced in cells expressing WT matriptase compared with control cells or cells expressing the catalytically inactive matriptase, suggesting conversion of the precursor form into smaller fragments (Fig. 4*A*). Moreover, no cleavage of GFP-APP695 was observed when HEK293 cells were transfected with matriptase and HAI-1, the physiological inhibitor of matriptase (supplemental Fig. S2) or with matriptase-2 (TMPRSS6), a close member of the matriptase subfamily (supplemental Fig. S3). Moreover, only the extracellular region of APP is involved in the matriptase processing event because a chimeric construct in which the transmembrane and cytoplasmic domains of APP695 (residues 624–695) were replaced with an equivalent domain of the unrelated type I membrane-bound protein LRP10 (residues 441–713) was also cleaved (supplemental Fig. S4B). These results support the exclusive role of the extracellular domain of APP in its processing by matriptase.

Given that active matriptase exists as a membrane-bound as well as a soluble shed entity (30), we next investigated whether an active soluble matriptase form could be involved in APP cleavage. Purified soluble matriptase or inactive S805A forms were exogenously added to the culture medium of HEK293 cells overexpressing GFP-tagged APP770, APP751, or APP695. A GFP-tagged APP fragment of 35 kDa was detected in the conditioned medium of all cells incubated with recombinant WT matriptase but not with matriptase S805A (Fig. 4*B*).

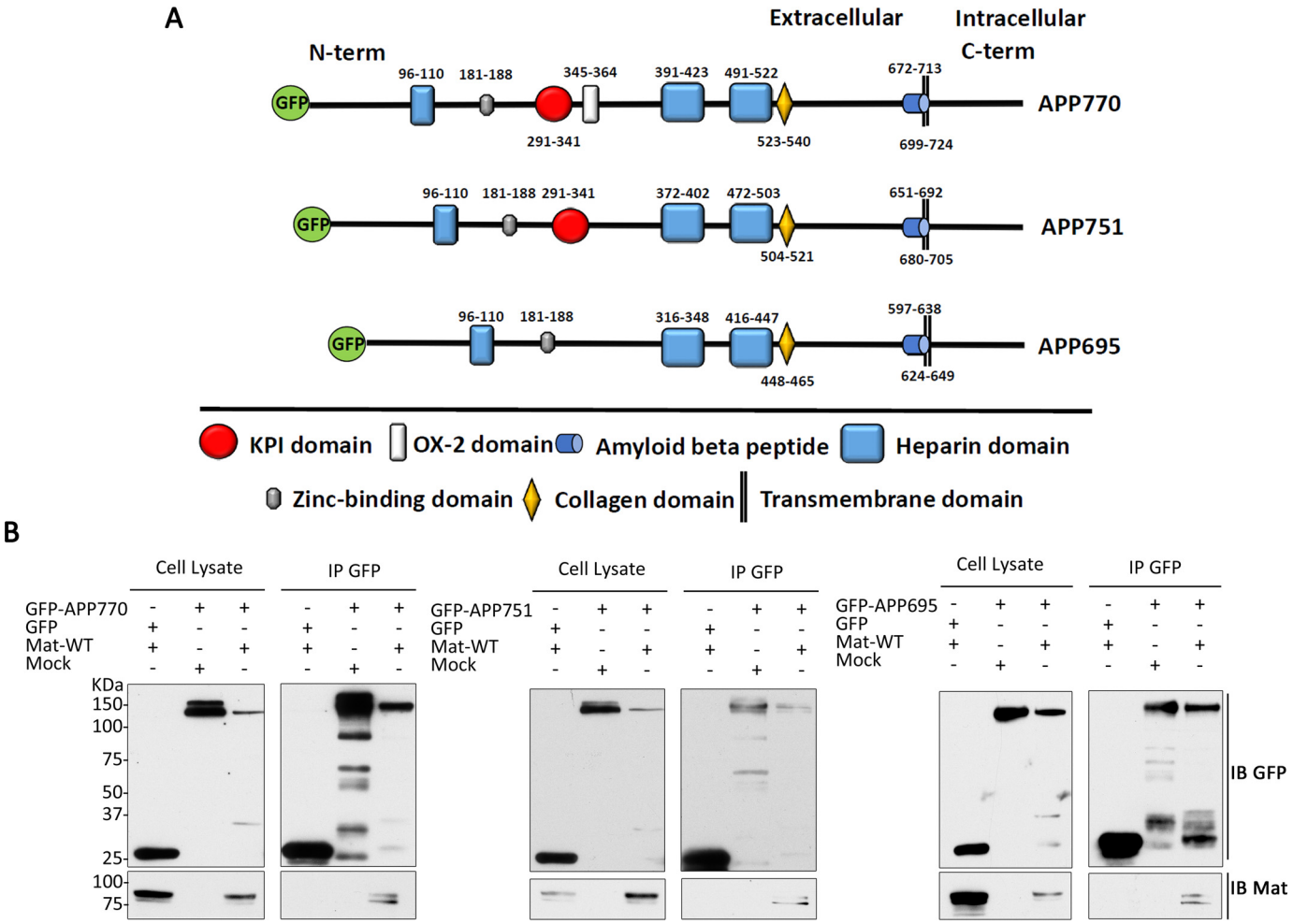

Figure 2. Matriptase interacts with APP770, APP751, and APP695. *A*, schematic representation of the GFP-tagged isoforms of APP. The structural elements of APP are depicted, including the heparin, KPI, OX-2, zinc-binding, collagen, amyloid *β*, and transmembrane domains. *B*, lysate of HEK293 cells transfected with matriptase and GFP-tagged APP770 (*left panel*), APP751 (*middle panel*), or APP695 (*right panel*) or with GFP were immunoprecipitated (*IP*) with GFP-Trap beads and then immunoblotted with anti-matriptase or anti-GFP antibodies to detect matriptase (*Mat*) and APP isoforms, respectively ($n = 3$ for each APP isoforms).

Concentration-dependent curves indicated that the cleavage of GFP-APP695 occurs at a concentration as low as 1 nM soluble matriptase (supplemental Fig. S5). These results suggest that soluble active matriptase can cleave APP isoforms in the pericellular space.

The physiological relevance of APP processing by matriptase was next analyzed with the human neuroblastoma SH-SY5Y cell line, which expresses endogenous APP695, APP751, and APP770 (31) but not matriptase (data not shown). SH-SY5Y cells were incubated with exogenous soluble WT matriptase or matriptase S805A as described above (Fig. 4*C*). Interestingly, a 10-kDa APP fragment was detected in the conditioned medium by Western blotting using an antibody against the N terminus of APP when cells were incubated with WT matriptase but not with the inactive recombinant matriptase S805A. This 10-kDa fragment would correspond to the portion of the APP extracellular N terminus fused to GFP (25 kDa) to form the 35 kDa fragment detected in the previous assays. This result confirms that soluble matriptase can cleave endogenous APP on SH-SY5Y cells.

To determine whether APP cleavage is due to a direct action of matriptase on APP and not from an indirect action of matriptase on another APP-cleaving enzyme, *in vitro* cleavage assays were performed with ^{35}S-labeled *in vitro* translated APP770, APP751, and APP695, and purified soluble WT matriptase or matriptase S805A (Fig. 4*D*). After incubation with increasing concentrations of purified soluble WT matriptase for 1 h at 37 °C, a reduction in the amount of full-length APP isoforms and an increased amount of APP fragments of around 50, 27, 20, and 10 kDa were detected by autoradiography. The higher molecular mass forms may correspond to intermediate processed fragments, but the 10 kDa fragment would correspond to the N-terminal APP fragment described in Fig. 4*C*. In contrast, no APP fragments were detected in the presence of inactive matriptase S805A (Fig. 4*D*). Together, these results suggest that matriptase directly cleaves the different APP isoforms and is not inhibited by the KPI domain of APP.

Identification of the precise matriptase cleavage site on APP

To identify the precise matriptase cleavage site on the APP extracellular domain, mass spectrometry (MS) analysis was performed on the APP fragments generated following the

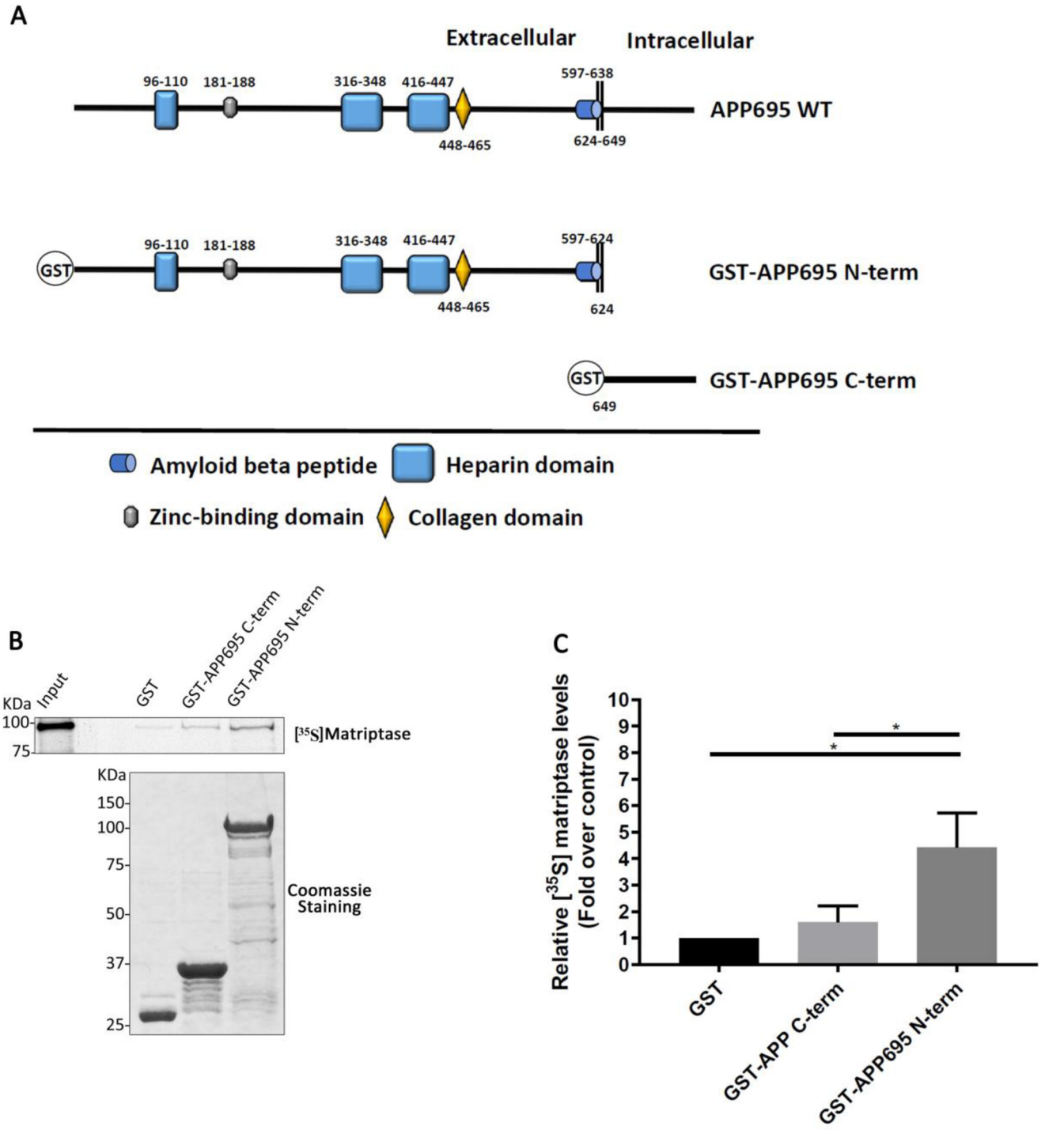

Figure 3. *In vitro* interaction of matriptase with the ectodomain of APP695. *A*, schematic representation of the GST-tagged APP695 deletion mutants used to determine the matriptase-binding domain. *B*, APP695 mutants and GST protein (10 μg) were immobilized on glutathione beads and incubated with *in vitro* translated ^{35}S-labeled matriptase. Bound proteins were separated by SDS-PAGE and detected by autoradiography. GST proteins were detected with Coomassie Blue staining. *Input*, 2.5% of the total *in vitro* translated product ($n = 6$). *C*, a Kruskal–Wallis test on the densitometric analysis of *B* was applied. There is a statistical difference between GST alone and GST-APP695 N-term and between GST-APP695 C-term and GST-APP695 N-term (*, $p < 0.05$). *Error bars* represent means ± S.D.

in vitro incubation of purified GST-APP695 N-term with or without soluble recombinant WT matriptase. Isolated GST-APP695 fragments were digested with chymotrypsin to produce several overlapping peptides, analyzed by HPLC coupled to an Orbitrap MS, and compared with purified GST-APP695 N-term alone (Fig. 5*A*). A main cleavage site for matriptase was identified at Arg-102 located on the first heparin domain of APP695 (Fig. 5*B*). This cleavage site is conserved in the different APP isoforms and would yield an N-terminal fragment with a predicted molecular mass of 12 kDa, consistent with the low-molecular-mass (10-kDa) APP fragment detected by immunoblotting and autoradiography

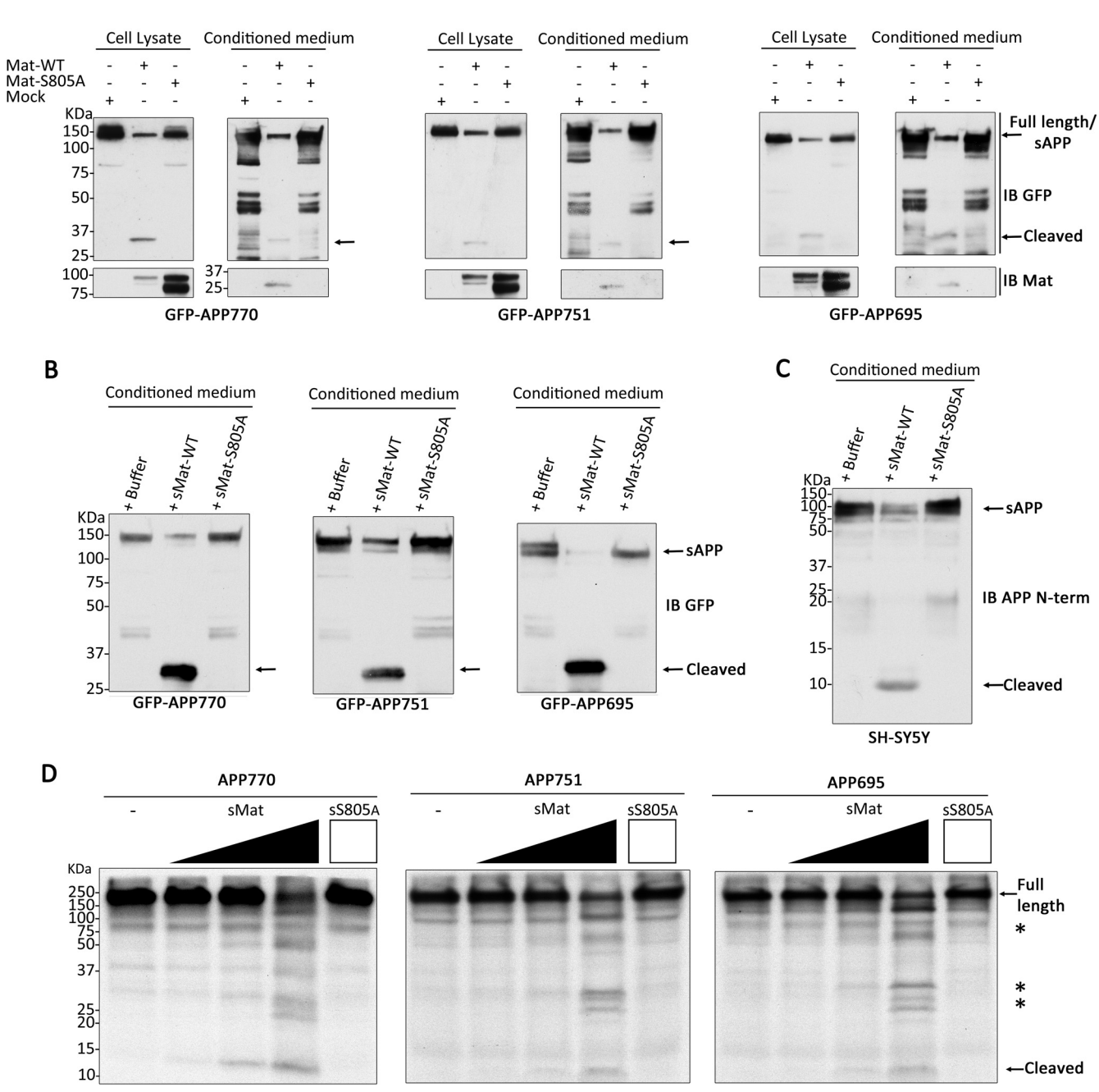

Figure 4. Matriptase cleaves APP770, APP751, and APP695 *in cellulo* and *in vitro*. *A*, HEK293 cells were transfected with WT matriptase (*Mat*), a catalytically inactive matriptase mutant (S805A), or empty vector (*Mock*) together with GFP-tagged APP770 (*left panel*), APP751 (*middle panel*), or APP695 (*right panel*). Lysates and conditioned media of these cells were immunoblotted (*IB*) with anti-matriptase or anti-GFP antibody to detect matriptase, APP isoforms, and APP fragments ($n = 3$ for each isoform). Note the GFP-tagged APP fragment (cleaved) of 35 kDa in cell lysate and medium (*arrow*). *B*, HEK293 cells transfected with GFP-tagged APP770 (*left panel*), APP751 (*middle panel*), or APP695 (*right panel*) were incubated without (*Buffer*) or with 5 nM recombinant WT matriptase (*sMat-WT*) or catalytically inactive matriptase mutant (*sMat-S805A*). Conditioned media were immunoblotted as described in *A*. *C*, SH-SY5Y cells expressing endogenous APP were incubated without (*Buffer*) or with 5 nM of recombinant WT matriptase (*sMat-WT*) or catalytically inactive matriptase mutant (*sMat-S805A*). Conditioned media were immunoblotted with anti-APP N-terminal antibody (22C11) to detect APP and APP fragments in the medium ($n = 3$). Note the APP fragment (cleaved) of 10 kDa. *D*, *in vitro* translated ^{35}S-labeled APP770 (*left panel*), APP751 (*middle panel*), and APP695 (*right panel*) were incubated with different concentrations (0, 1, 10, and 100 nM) of recombinant WT matriptase (*sMat*) or 100 nM catalytically inactive matriptase mutant (*sS805A*) for 1 h at 37 °C. Reaction products were separated by SDS-PAGE and detected by autoradiography ($n = 3$). Note the APP fragment (cleaved) of 10 kDa (*arrow*) and other higher molecular mass fragments (*asterisks*) in the presence of recombinant WT matriptase.

when APP695, APP751, and APP770 were incubated with matriptase (see Fig. 4). To confirm this cleavage site, Arg-102 was mutated to Ala (R102A) in GFP-tagged APP695. HEK293 cells expressing either GFP-tagged APP695 WT or R102A were incubated for 16 h with purified soluble WT matriptase (Fig. 5*C*). Expression of the R102A mutant abolished the formation of the 35-kDa GFP-APP695 fragment, indicating that this mutant is resistant to cleavage by matriptase. Together, these results indicate that Arg-102 is the main matriptase cleavage site in the ectodomain of APP.

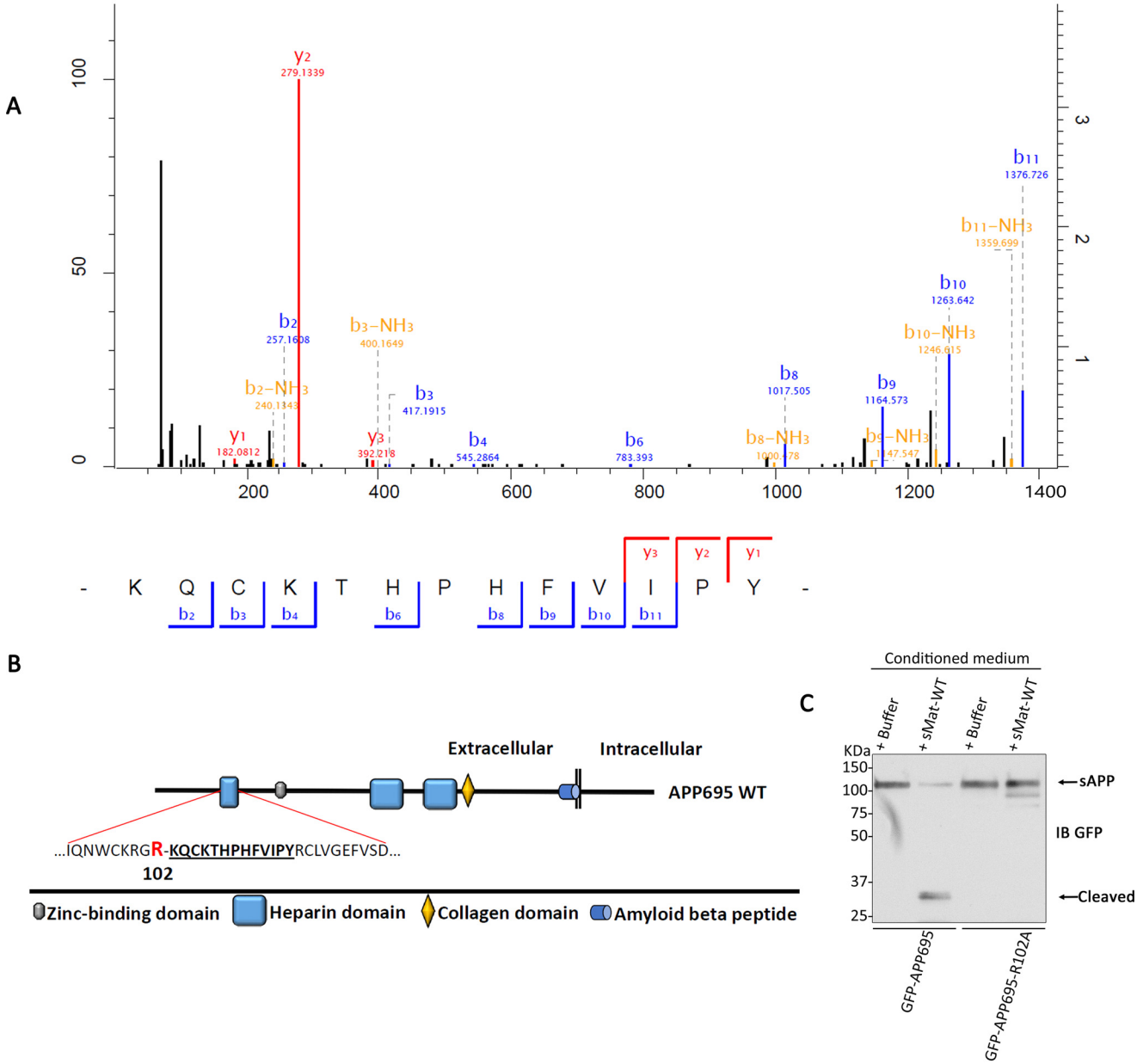

Figure 5. Matriptase cleaves APP at arginine 102. *A*, tandem mass spectrometry spectra from peptide ion trap collision-induced dissociation fragmentation for the peptide KQCKTHPHFVIPY identified after *in vitro* digestion and LC-MS/MS analysis of GST-APP695 ectodomain fragments generated by matriptase cleavage. Shown is a representative annotated MS/MS fragmentation spectrum with the identified matched N terminus-containing ions (b ions) in *blue* and the C terminus-containing ions (y ions) in *red*. Peptide intensities were summarized per amino acid residue and plotted in relation to each other. The detected peptide sequences indicate that Arg-102 is the main cleavage site. *B*, schematic representation of the position of the Arg cleaved by matriptase in the ectodomain of APP695 tagged with GST that was used to determine the matriptase cleavage site in *A*. *C*, HEK293 cells transfected with GFP-tagged APP695 wild type or in which Arg-102 was mutated to Ala (APP695 R102A) were incubated without (*Buffer*) or with 5 nM recombinant WT matriptase (*sMat-WT*). Conditioned media were immunoblotted (*IB*) with anti-GFP antibody to detect sAPP and APP fragments ($n = 3$). Note the absence of the GFP-tagged APP fragment (cleaved) of 35 kDa in the GFP-APP695 R102A lanes.

Matriptase processing of APP alters Aβ40 production

Given that the cleavage of APP by proteases has been previously shown to result in an alteration of Aβ peptide formation (32, 33), we next determined whether matriptase cleavage has an effect on the endogenous APP processing pathway leading to Aβ formation (Fig. 6). SH-SY5Y cells were incubated with or without exogenous, purified soluble WT matriptase or matriptase S805A for 36 h, and ELISAs were performed on the culture medium to specifically quantify the accumulation of Aβ40 peptide. A 72% decrease ($p \leq 0.001$) in Aβ40 levels was observed in cells incubated with WT matriptase compared with control cells (without matriptase) or cells incubated with matriptase S805A (Fig. 6*A*). These results suggest that matriptase cleavage reduces APP processing into Aβ40 in SH-SY5Y cells.

To determine whether the alteration of Aβ40 production involved the Arg-102 matriptase cleavage site in APP, Aβ40 levels were measured in the culture medium of HEK293 cells transfected with GFP-tagged APP695 WT or APP695 R102A mutant with or without matriptase (Fig. 6*B*). As observed in SH-SY5Y incubated with exogenous purified soluble WT

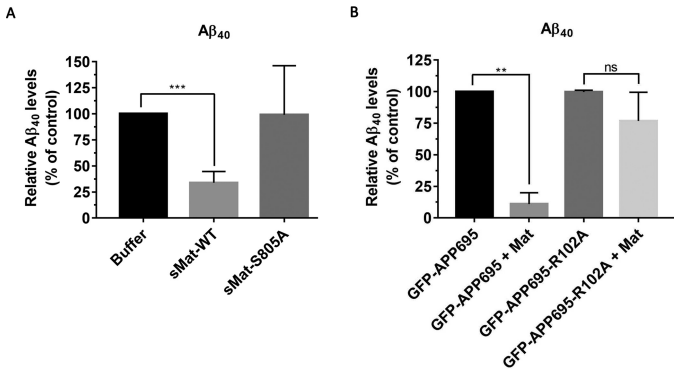

Figure 6. Matriptase cleavage of APP at Arg-102 alters Aβ40 production. *A*, SH-SY5Y cells were incubated without (*Buffer*) and with 5 nM recombinant WT matriptase (*sMat-WT*) or catalytically inactive matriptase mutant (*sMat-S805A*). Conditioned media were collected after 36 h, and Aβ40 levels were analyzed by ELISA. *Error bars* represent means ± S.D. Results are expressed as means ± S.D. ($n = 3$) and are normalized to the protein concentration in the medium. ***, $p < 0.001$. *B*, HEK293 cells transfected with GFP-tagged APP695 wild type or in which Arg-102 was mutated to Ala (APP695 R102A) and without or with matriptase (*Mat*). Aβ40 levels in the conditioned media were analyzed by ELISA as described in *A*. **, $p < 0.05$; *ns*, not significant.

matriptase (Fig. 6*A*), a 90% decrease of Aβ40 levels ($p \leq 0.01$) was quantified in HEK293 cells expressing APP695 with matriptase (Fig. 6*B*). In contrast, the level of Aβ40 was not altered in cells expressing APP695 R102A with or without matriptase compared with cells expressing APP695 WT without matriptase (Fig. 6*B*). These results suggest that the cleavage of APP at Arg-102 by matriptase affects the processing of APP by secretases in turn to reduce Aβ40 production.

Discussion

Recent advances have reinforced the hypothesis that accumulation of Aβ is the main initiator of AD. Therefore, identifying factors that influence/regulate APP processing into Aβ is crucial in understanding AD pathogenesis and designing novel therapeutic strategies. In this study, we have identified matriptase as a novel protease expressed in human brain tissue that cleaves APP in its ectodomain, which causes a significant reduction in the production of Aβ40. Importantly, this suggests a potential neuroprotective role of matriptase in the APP processing events leading to Aβ production.

Matriptase, one of the best characterized TTSPs, is known to be mostly expressed in epithelial cells where it carries out essential functions in development, differentiation, and maintenance of epithelial barrier integrity (27). Interestingly, matriptase has been recently reported to be expressed in non-epithelial cells, more specifically in mouse neural stem/progenitor cells and neurons as well as in mouse cortex, hippocampus, striatum, and subventricular zone. Its expression has also been associated with mouse neuronal development, migration, and differentiation (21, 22). In this study, we demonstrate for the first time that matriptase mRNA is present in the frontal and temporal cortex, hippocampus, and cerebellum of the human brain. The expression levels of matriptase mRNA observed between the different human brain regions tested were similar to those detected in mouse brain regions (22). By analysis of whole transcriptome data sets deposited in the European Nucleotide Archive, we found very low levels of matriptase mRNA in human fetal brains, but a sharp increase in levels was observed in the DLPC of young individuals followed by a constant decrease during aging. The DLPC is an area of the brain involved in executive functions that undergoes the greatest amount of postnatal development that lasts until adulthood (34–36). Thus, the matriptase expression pattern in this brain area potentially follows a specific temporal pattern during brain development and neurogenesis and may explain why low matriptase mRNA levels were detected in older individuals.

Interestingly, of all brain cells tested, neurons showed the highest level of matriptase mRNA, similar to that found in human epithelial colorectal adenocarcinoma Caco-2/15 cells, a low invasive colon cancer cell line, but that level was 100 times lesser than levels found in HCT116 cells, a highly invasive colon cancer cell line. These data indicate that human neurons express matriptase mRNA and support the idea that matriptase has important physiological functions in these cells.

Our attempts to detect matriptase protein expression in human brain tissues or neurons from adult/elderly individuals were unsuccessful, which may be due to antibody sensitivity but may also be due to temporal regulation of matriptase expression with transcripts at their highest expression levels soon after birth and significantly lower in brains of older individuals (Fig. 1*D*). However, we detected matriptase protein expression in hiPSCs after 6 weeks of neuronal differentiation but not in undifferentiated cells. The detection of matriptase in human neuronal cells derived from iPSCs is novel and is in accordance with previous results obtained by others with mouse neuronal progenitor cells (22) and by our group with mouse astrocytes (supplemental Fig. S6). Overall, although matriptase levels may be low and particularly difficult to detect in adult brain tissues, they could be sufficient for physiological relevance. The presence of matriptase in human brain cells could also have a pathophysiological effect such as in cancer progression. In many tumors, matriptase RNA/protein levels are up-regulated, and there is a positive correlation between matriptase expression and tumor grade (37–40). Additionally, the expression of HAI-1, an endogenous inhibitor of matriptase, whose expression in the human brain is well-documented (41, 42), is often deregulated in human cancer (39). Indeed, overexpression of HAI-1 has been reported to suppress the *in vitro* invasive capability of human glioblastoma cells (41). Therefore, identification of the different proteolytic substrates of matriptase in brain cells will help delineate its basic function in the central nervous system and its implication in various neurological diseases.

We found that matriptase interacts with and cleaves all three major APP isoforms, indicating that the KPI domain found in APP751 and APP770 is not crucial for this interaction and does not inhibit matriptase. These results differ from those reported for matriptase-2 (also named TMPRSS6), a close member of the matriptase subfamily. The intact KPI domain of APP770 and APP751 was shown to be important for the interaction with matriptase-2 and to inhibit its enzymatic activity (25). Taken together, these results may be explained by the differences in the catalytic domain of matriptase and matriptase-2 (45% homology) and in their protein–protein interaction domains, which are key for their respective activity and substrate speci-

ficities (43). Moreover, the amino acid sequence of the APP KPI domain also differs from that of the KPI domain of HAI-1. The canonical active site of HAI-1 that interacts with the second negatively charged binding site in the catalytic domain of matriptase was identified as Arg-258 and Arg-260 (44). Comparison of the Kunitz sequences of APP770/751 and HAI-1 indicates that Arg-258 of HAI-1 is replaced by a proline in the APP Kunitz domain, which could significantly hinder its interaction with the active site of matriptase.

Matriptase hydrolyzes peptide bonds C-terminal to specific basic amino acids with a clear preference for Arg over Lys in the P1 position and basic amino acids in the P3 position (18, 43). Accordingly, mass spectrometry analysis identified Arg-102 within the sequence KRGR ↓ KQCK in the first heparin domain of the extracellular region of APP as the main matriptase cleaving site. The three-dimensional structure of residues 18–123 of this heparin domain (Protein Data Bank code 1MWP) reveals that Arg-102 is well-exposed at the surface of the protein and thus accessible for cleavage by a protease. To our knowledge, this specific Arg has never been identified as a cleavage site for other proteases. Interestingly, the residues that form the structural network in the heparin domain are conserved between the E1 domain of APP and amyloid precursor-like protein 2 (APLP2) but not APLP1 (45), suggesting that APLP2 may also be a potential matriptase substrate.

Enzymatically active matriptase exists as a membrane-bound as well as an extracellular soluble, shed form (46, 47). Consequently, both forms can interact with APP and cleave its ectodomain. Using purified soluble matriptase applied on SH-SY5Y cells (which do not express matriptase), we showed that endogenous APP is cleaved, suggesting that shed matriptase originating from expression in either homologous or adjacent cells can process APP and therefore impact the physiological function of APP. Recent evidence suggests that the ectodomain of APP and its proteolytic fragments are important for its biological roles such as cell growth, cell adhesion and motility, neurite outgrowth, and cell survival (48, 49). For example, the first heparin domain in the APP N terminus, which contains the Arg-102 matriptase cleavage site, interacts with the extracellular matrix through heparan sulfate proteoglycans and is involved in the regulation of neurite outgrowth (50). Moreover, both APP and matriptase activities were reported to be involved in the migration and differentiation of mouse neuronal precursors (22, 51). Whether matriptase cleavage alters these different APP functions will need to be elucidated.

N-terminal processing of APP may influence the cleavage efficiency toward Aβ production. In the last few years, many proteases (other than α- and β-secretases) have been reported to cleave the APP ectodomain and alter Aβ production. These include the membrane type 5 matrix metalloproteinase, referred to as η-secretase, which cleaves APP at residue 504 (APP695 numbering) and releases a long truncated ectodomain (sAPPη) as well as a membrane-bound CTFη that is further cleaved by α- and β-secretases, releasing Aη peptides that alter neuronal activity and plasticity (52). The asparagine endopeptidase has also been reported to act as a novel δ-secretase by cleaving APP at Asn-373 and Asn-585 residues, selectively influencing the rate of β-secretase cleavage and promoting Aβ production (33). In a similar way, we showed that matriptase cleaves APP at Arg-102, causing a significant decrease (>70%) of Aβ40 levels, which was completely abolished when Arg-102 was replaced by Ala (APP R102A), indicating that the matriptase-specific cleavage affects APP processing by secretases in turn to reduce Aβ40 production. Interestingly, the matriptase cleavage site is located in a highly flexible loop region (residues 98–105) shown to be important for APP dimerization and processing into Aβ (53, 54). Indeed, biochemical data revealed that addition of a synthetic peptide corresponding to this loop region interferes with APP dimerization and decreases the generation of sAPPβ and Aβ when added to neuroblastoma SH-SY5Y cells (54), indicating a direct or indirect influence of dimerization on APP processing by β-secretases. On this basis, we propose that matriptase proteolytically cleaves the APP ectodomain, potentially impairing APP dimerization and interaction with secretases, which would reduce the rate of Aβ production.

Despite large-scale efforts to therapeutically target the putative disease mechanisms in AD, neuroprotective treatments are still lacking. Presently, β- and γ-secretases are prime therapeutic targets under development, but many concerns have been recently raised as to how effective these particular enzymes are as therapeutic targets (55, 56). Therefore, there is growing consensus that gaining a better understanding of the regulation of APP processing is crucial for identifying new potential therapies to reduce Aβ accumulation and combat AD. Our findings describe a new cleavage of APP by matriptase that reduces the production of Aβ peptide probably by altering the processing by secretases. These observations suggest that matriptase may have a neuroprotective role in controlling the levels of Aβ peptide. Conversely, low levels of matriptase observed in aging brain as well as impaired matriptase activity or HAI-1 levels could accelerate the formation of amyloid plaque and the progression of the disease. Our findings highlight a previously unappreciated role of matriptase in human brain, and future studies will aim to clarify its role in physiological and pathophysiological functions of APP.

In conclusion, this study identifies matriptase as a novel APP-cleaving protease and furthers our understanding of APP biology. Future experiments will be needed to validate the biological relevance of matriptase-mediated APP processing *in vivo* and its potential role in the onset of AD pathology.

Experimental procedures

Antibodies and reagents

Anti-GFP rabbit polyclonal antibodies were purchased from Clontech Molecular Probes (Eugene, OR), anti-human matriptase polyclonal antibodies were from Bethyl Laboratories (Montgomery, TX), and anti-APP N-terminal 22C11 mAbs were from EMD Millipore (Billerica, MA).

DNA constructs

Mammalian expression vectors GFP-APP695 and GST-APP695 C-term (residues 647–695) were kindly provided by Dr. Ritva Tikkanen (University Clinic of Frankfurt, Germany). The APP695 fragment containing the N terminus (residues

20–612) was subcloned in pET41a (Novagen). The recombinant matriptase (residues 596–855) construct used for bacterial expression (pQE30 vector, Qiagen, Mississauga, Ontario, Canada) and S805A matriptase pcDNA3.1 have been described previously (29, 57). Human APP770 was kindly provided by Dr. Christian Haass (Ludwig Maximilians University, Munich, Germany), and APP751 was purchased from SinoBiological Inc. (Beijing Economic and Technological Development Area, Beijing, China); both were subcloned in pcDNA3.1 and pCMV5-GFP. All constructs were sequenced before use.

Cell culture

HEK293 and Caco-2/15 cells were kindly provided by Dr. Alexandra Newton (University of California, San Diego, La Jolla, CA) and Dr. Jean-Francois Beaulieu (Université de Sherbrooke), respectively. HEK293 cells were grown in Dulbecco's modified Eagle's high-glucose medium (Invitrogen) containing 10% fetal bovine serum (FBS) (Hyclone Laboratories, Logan, UT), 2 mM L-glutamine, 50 IU/ml penicillin, and 50 μg/ml streptomycin (Wisent, St-Bruno, Quebec, Canada). HEK293 cells were transfected with Lipofectamine 2000 transfection reagent (Invitrogen) according to the manufacturer's instructions. HCT 116 cells (ATCC CCL-247) from American Type Culture Collection (Manassas, VA) were grown in McCoy's 5A medium (Invitrogen) containing 10% FBS, 2 mM L-glutamine, 50 IU/ml penicillin, and 50 μg/ml streptomycin. Caco-2/15 cells were grown in Eagle's minimum essential medium (Invitrogen) with 20% fetal bovine serum, 2 mM L-glutamine, 50 IU/ml penicillin, and 50 μg/ml streptomycin. SH-SY5Y cells (ATCC CRL-2266) were purchased from ATCC and grown in minimum Eagle's medium:Ham's F-12 (1:1) (Invitrogen) containing 10% FBS, 2 mM sodium pyruvate (Invitrogen), 2 mM L-glutamine, 50 IU/ml penicillin, and 50 μg/ml streptomycin.

Coimmunoprecipitation

HEK293 cells were plated in 60-mm culture dishes and transfected with the indicated constructs. After 48 h, the cells were washed twice with phosphate-buffered saline; lysed in 50 mM Tris buffer (pH 7.4) containing 150 mM NaCl, 1% Triton X-100, and protease inhibitors for 1 h at 4 °C; and then centrifuged at 15,000 × *g* for 20 min. The cleared supernatants were incubated with GFP-Trap®_A (Chromotek, Germany) overnight at 4 °C and washed with 10 mM Tris/HCl (pH 7.5), 150 mM NaCl, 0.5 mM EDTA buffer three times. Bound immune complexes were boiled in Laemmli sample buffer and analyzed by SDS-PAGE and immunoblotting.

Immunoblotting

The protein samples were separated by 10 or 16% SDS-polyacrylamide gel electrophoresis (PAGE) and transferred to 0.45-μm-diameter pore-size nitrocellulose membranes (PerkinElmer Life Sciences). The membranes were blocked in Tris-buffered saline (20 mM Tris-HCl (pH 7.4) and 150 mM NaCl) containing 0.1% Tween 20 and 5% nonfat dry milk, incubated with primary antibodies for 1 h at room temperature, subsequently incubated with horseradish peroxidase-conjugated goat anti-rabbit or anti-mouse IgG for 1 h at room temperature (Bio-Rad), and enhanced using a chemiluminescence detection reagent (Pierce).

Glutathione S-transferase pulldown assays

GST fusion proteins were expressed in *Escherichia coli* BL21 and purified on glutathione-Sepharose 4B beads (GE Healthcare) according to the manufacturer's instructions. The ^{35}S-labeled *in vitro* translation products of pcDNA3.1-human APP770, APP751, APP695, and matriptase were prepared using the TnT T7 rabbit reticulocyte Quick Coupled Transcription/Translation system (Promega, San Luis Obispo, CA) in the presence of EasyTag EXPRESS^{35}S labeling mixture (73% Met and 22% Cys; 41,000 Ci/mmol; PerkinElmer Life Sciences). A total of 5–10 mg of purified GST or GST fusion protein was incubated with the *in vitro* translated products in 20 mM Tris-HCl buffer (pH 7.4) containing 150 mM NaCl, 1% Triton X-100, and protease inhibitors for 2h at 4 °C. Beads were washed four times with the same buffer. Bound proteins were eluted with Laemmli buffer, resolved by SDS-PAGE, and visualized by autoradiography.

In vitro cleavage assays

WT matriptase (residues 596–855) and S805A mutant were produced and purified as described previously (57). The ^{35}S-labeled *in vitro* translation products of pcDNA3.1-human APP770, APP751, and APP695 were prepared as described under "Glutathione *S*-transferase pulldown assays." Enzymatic assays were performed in a final volume of 100 μl in 100 mM Tris-HCl (pH 8.5) containing 500 μg/ml BSA. *In vitro* translated ^{35}S-labeled APP isoforms (0.5 μl) were incubated with 0, 1, 10, and 100 nM recombinant WT matriptase or 100 nM of inactive matriptase S805A for 1 h at 37 °C. Enzymatic reactions were stopped by the addition of 30 μl of Laemmli buffer, resolved by SDS-PAGE, and visualized by autoradiography.

Treatment of cells with recombinant matriptase

Culture medium of HEK293 or SH-SY5Y cells was removed and replaced with 2 ml of serum-free HCELL-100 medium (Wisent, St-Bruno, Quebec, Canada) containing different concentrations (0–100 nM) of recombinant soluble human WT matriptase or mutant S805A. After a 36-h incubation, the conditioned medium was collected and either concentrated with Amicon Ultra centrifugal filters (3,000 nominal molecular weight limit (Merck Millipore Ltd.) for immunoblotting or directly used for ELISA analysis. Cells were lysed in 50 mM Tris buffer (pH 7.4) containing 150 mM NaCl, 1% Triton X-100, and protease inhibitors for 1 h at 4 °C. Both conditioned medium and cell lysate were boiled in Laemmli sample buffer and analyzed by SDS-PAGE and immunoblotting.

ELISA quantification of Aβ40

For ELISAs, SH-SY5Y cell were seeded at a density of 2×10^6 cells in 60-mm culture dishes and allowed to grow to >75% confluence. HEK293 cells were seeded at a density of 1.5×10^6 cells in 60-mm culture dishes and transfected as described under "Coimmunoprecipitation." When the cells reached the desired density, the medium was removed and replaced with conditioned medium containing matriptase WT or S805A as

described under "Treatment of cells with recombinant matriptase." After a 48-h incubation, the supernatants were harvested, and Aβ40 levels were quantified using an Amyloid β40 Human ELISA kit (KHB3481, Invitrogen) according to the manufacturer's instructions. An Infinite M200 Plate reader (Tecan) was used to detect the signal. The Aβ40 concentrations were determined by comparison with the standard curve and normalized to total protein concentration in the medium.

Human brain tissues and human cell total RNA

Human frontal cortex, temporal, hippocampal, and cerebellum samples were obtained from the Douglas Hospital Brain Bank in Montreal, Quebec, Canada. The mean age at death was 73.8 $\pm$ 12.1 years. The post-mortem interval was 22.3 $\pm$ 7.4 h. Control cases had a clinical diagnosis of non-demented elderly patients. Total RNAs from human neuron, astrocyte, microvascular endothelial cell, choroid plexus epithelial cell, and Schwann cell were purchased from 3H Biomedical (Uppsala, Sweden).

Tissue RNA isolation and quantitative real-time RT-PCR

Total RNA extractions were performed on cell pellets using TRIzol (Invitrogen) with chloroform following the manufacturer's protocol. The aqueous layer was recovered, mixed with 1 volume of 70% ethanol, and applied directly to an RNeasy Mini kit column (Qiagen). DNase treatment on the column and total RNA recovery were performed according to the manufacturer's protocol. RNA quality and the presence of contaminating genomic DNA were verified as described previously (58). RNA integrity was assessed with an Agilent 2100 Bioanalyzer (Agilent Technologies). Reverse transcription was performed on 1.1 μg of total RNA with Transcriptor reverse transcriptase, random hexamers, dNTPs (Roche Diagnostics), and 10 units of RNaseOUT (Invitrogen) following the manufacturer's protocol in a total volume of 10 μl. All forward and reverse primers were individually resuspended to 20–100 μM stock solutions in Tris-EDTA buffer (Integrated DNA Technologies, Inc.) and diluted as a primer pair to 1 μM in RNase DNase-free water (Integrated DNA Technologies, Inc.). Real-time qPCRs were performed in 10 μl in 96-well plates on a CFX-96 thermocycler (Bio-Rad) with 5 μl of 2$\times$ iTaq Universal SYBR Green Supermix (Bio-Rad), 10 ng (3 μl) of cDNA, and 200 nM (final concentration; 2 μl) primer pair solutions. The following cycling conditions were used: 3 min at 95 °C and 50 cycles of 15 s at 95 °C, 30 s at 60 °C, and 30 s at 72 °C. Relative expression levels were calculated using the qBASE framework (59) and the housekeeping genes *YWHAZ*, *GAPDH*, and *SDHA* for human cDNA. Primer design and validation were evaluated as described elsewhere (58). In every qPCR run, a no-template control was performed for each primer pair, and these were consistently negative. All primer sequences are available in supplemental Table S1.

Differentiation of human induced pluripotent stem cells into cortical neurons

The differentiation protocol was based on a previous study (60). However, the Noggin agonist LDN193189 was used to reduce the recombinant Noggin concentration. The hiPSCs were dissociated using Accutase (Innovative Cell Technology, San Diego, CA) and plated on growth factor-reduced Matrigel (Corning) in PeproGrow human ES cell medium (PeproTech) supplemented with 10 μM ROCK (Rho-associated, coiled-coil–containing protein kinase) inhibitor (Y-27632; 10 μM; Cayman Chemical). When 70% cell confluence was reached, the medium was changed to defined default medium (61) supplemented with B27 (1$\times$ final), 10 ng/ml Noggin (PeproTech,) and 0.5 μM LDN193189 (Sigma). The medium was changed every day. After 16 days of differentiation, the medium was changed to defined default medium/B27 and replenished every day. At day 24, neural progenitors were manually detached from the plate and plated on growth factor-reduced Matrigel-coated plates or chamber slides (LabTek). Five days after dissociation, half of the medium was exchanged for Neurobasal A medium supplemented with B27 (1$\times$ final) and changed again every 3 days.

Analysis of public RNA-seq data sets

RNA sequences were obtained from a previously published study on human brain development (28). Briefly, sequences from deep-frozen post-mortem brain tissues from 39 individuals without neurological or psychiatric illnesses were retrieved from the European Nucleotide Archive (http://www.ebi.ac.uk/ena).[4] All samples are from DLPC gray matter (Brodmann area 9/46) spanning from fetal life to the eighth decade of life. Fetal tissue was taken from the prefrontal region over the dorsal convexity of the frontal lobe just anterior to the temporal pole. Run accession numbers used are listed in supplemental Table S2. The obtained paired-end reads from RNA-seq data sets were aligned to the human reference genome GRCh37/hg19 using HISAT2 (version 2.03) (62). The number of reads mapping to each gene was calculated with featureCount version 1.4.6.p5 (63) using the annotated transcriptome from Ensembl (http://www.ensembl.org/Homo_sapiens/Info/Index). Normalization of gene expression was obtained by calculating fragments per kilobase of exon per million fragments mapped for each RNA-seq sample (supplemental Table S2).

Mass spectrometry analysis

GST fusion proteins were expressed in *E. coli* BL21 and purified on glutathione-Sepharose 4B beads according to the manufacturer's instructions. Bound proteins were incubated for 2 h at 37 °C in a volume of 100 μl of 100 mM Tris-HCl (pH 8.5) containing or not 100 nM recombinant soluble WT matriptase. The supernatant was then collected, lyophilized, and suspended in 25 μl of 10 mM HEPES/KOH (pH 7.5). Proteins were reduced with 3.24 mM DTT and alkylated with 13.5 mM iodoacetamide. The urea concentration was lowered to 1 M with the addition of 50 mM ammonium bicarbonate (NH_4HCO_3) and 1 mM $CaCl_2$ and digested with chymotrypsin (Thermo Scientific, catalogue number 90056). Digested samples were desalted with C_{18} tip (Thermo Scientific, catalogue number 87764), lyophilized, and resuspended in 1% formic acid prior to mass spectrometry analysis. Chymotrypsin-digested peptides were separated using a Dionex UltiMate 3000 nano-

[4] Please note that the JBC is not responsible for the long-term archiving and maintenance of this site or any other third party-hosted site.

HPLC system. Ten microliters of sample (a total of 2 μg) in 1% (v/v) formic acid was loaded with a constant flow of 4 μl/min onto an Acclaim PepMap100 C_{18} column (0.3-mm inner diameter × 5 mm; Dionex Corp., Sunnyvale, CA). After trap enrichment, peptides were eluted off onto a PepMap C_{18} nanocolumn (75 μm × 50 cm; Dionex Corp.) with a linear gradient of 5–35% solvent B (90% acetonitrile with 0.1% formic acid) over 240 min with a constant flow of 200 nl/min. The HPLC system was coupled to an Orbitrap QExactive mass spectrometer (Thermo Fisher Scientific Inc.) via an EasySpray source. The spray voltage was set to 2.0 kV, and the temperature of the column was set to 40 °C. Full-scan MS survey spectra (m/z 350–1600) in profile mode were acquired in the Orbitrap with a resolution of 70,000 after accumulation of 1,000,000 ions. The 10 most intense peptide ions from the preview scan in the Orbitrap were fragmented by collision-induced dissociation (normalized collision energy of 35% and resolution of 17,500) after the accumulation of 50,000 ions. Maximal filling times were 250 ms for the full scans and 60 ms for the MS/MS scans. Precursor ion charge state screening was enabled, and all unassigned charge states as well as singly, septuply, and octuply charged species were rejected. The dynamic exclusion list was restricted to a maximum of 500 entries with a maximum retention period of 40 s and a relative mass window of 10 ppm. The lock mass option was enabled for survey scans to improve mass accuracy. Data were acquired using Xcalibur software. Data were processed, searched, and quantified using the MaxQuant software package version 1.5.2.8 using the human UniProt database (July 16, 2013; 88,354 entries).

Quantification and bioinformatics analysis

The settings used for the MaxQuant analysis were as follows: five miscleavages were allowed; trypsin (Lys/Arg not before Pro) and chymotrypsin (Leu/Phe/Trp/Tyr not before Pro) were used; variable modifications included in the analysis were methionine oxidation and protein N-terminal acetylation. A mass tolerance of 7 ppm was used for precursor ions, and a tolerance of 20 ppm was used for fragment ions. To achieve reliable identifications, all proteins were accepted based on the criterion that the number of forward hits in the database was at least 95-fold higher than the number of reverse database hits, thus resulting in a false discovery rate of less than 5%.

Statistical analysis

Experiments were performed at least in triplicate, and results are expressed as means ± S.D. The statistical significance of differences between samples was assessed using an unpaired two-tailed student t test, Kruskal–Wallis test, or a two-tailed Spearman non-parametric correlation. A p value <0.05 was considered significant.

Author contributions—E. L. planned and performed most of the experiments, collected and analyzed the data, made all the figures, and drafted the manuscript. A. D. and F. B. performed experiments, provided experimental advice, and revised the manuscript. A. F., G. B., S. M., and D. G. performed experiments and revised the manuscript. C. L. and R. L. designed the study, provided intellectual feedback, participated in interpretation of data, and revised the manuscript. All authors read and approved the final version of the manuscript and agree to be accountable for all aspects of the work.

Acknowledgments—We thank Dr. Ritva Tikkanen (University of Giessen, Germany) for the generous gift of GFP-APP695 and GST-APP695 C-term constructs and Dr. Christian Haass (Ludwig Maximilians University, Munich, Germany) for APP751 cDNA. We also thank the Douglas Hospital Brain Bank for providing human brain tissues and the Laboratoire de Génomique Fonctionnelle de l'Université de Sherbrooke and the Plateforme de Protéomique de l'Université de Sherbrooke for RT-qPCR and MS analysis, respectively. We are grateful to Sébastien Dion for the purification of soluble matriptase and to Dr. Jean-François Beaulieu (Université de Sherbrooke) for the Caco2/15 cells.

References

1. Chiang, P. K., Lam, M. A., and Luo, Y. (2008) The many faces of amyloid β in Alzheimer's disease. *Curr. Mol. Med.* **8,** 580–584
2. Arai, H., Lee, V. M., Messinger, M. L., Greenberg, B. D., Lowery, D. E., and Trojanowski, J. Q. (1991) Expression patterns of β-amyloid precursor protein (β-APP) in neural and nonneural human tissues from Alzheimer's disease and control subjects. *Ann. Neurol.* **30,** 686–693
3. Kitaguchi, N., Takahashi, Y., Tokushima, Y., Shiojiri, S., and Ito, H. (1988) Novel precursor of Alzheimer's disease amyloid protein shows protease inhibitory activity. *Nature* **331,** 530–532
4. Schmaier, A. H., Dahl, L. D., Rozemuller, A. J., Roos, R. A., Wagner, S. L., Chung, R., and Van Nostrand, W. E. (1993) Protease nexin-2/amyloid β protein precursor. A tight-binding inhibitor of coagulation factor IXa. *J. Clin. Investig.* **92,** 2540–2545
5. Preece, P., Virley, D. J., Costandi, M., Coombes, R., Moss, S. J., Mudge, A. W., Jazin, E., and Cairns, N. J. (2004) Amyloid precursor protein mRNA levels in Alzheimer's disease brain. *Brain Res. Mol. Brain Res.* **122,** 1–9
6. Johnson, S. A., McNeill, T., Cordell, B., and Finch, C. E. (1990) Relation of neuronal APP-751/APP-695 mRNA ratio and neuritic plaque density in Alzheimer's disease. *Science* **248,** 854–857
7. Sun, X., He, G., and Song, W. (2006) BACE2, as a novel APP θ-secretase, is not responsible for the pathogenesis of Alzheimer's disease in Down syndrome. *FASEB J.* **20,** 1369–1376
8. Grau, S., Baldi, A., Bussani, R., Tian, X., Stefanescu, R., Przybylski, M., Richards, P., Jones, S. A., Shridhar, V., Clausen, T., and Ehrmann, M. (2005) Implications of the serine protease HtrA1 in amyloid precursor protein processing. *Proc. Natl. Acad. Sci. U.S.A.* **102,** 6021–6026
9. Park, H.-J., Kim, S.-S., Seong, Y.-M., Kim, K.-H., Goo, H. G., Yoon, E. J., Min, D. S., Kang, S., and Rhim, H. (2006) β-Amyloid precursor protein is a direct cleavage target of HtrA2 serine protease. Implications for the physiological function of HtrA2 in the mitochondria. *J. Biol. Chem.* **281,** 34277–34287
10. Lu, P., Takai, K., Weaver, V. M., and Werb, Z. (2011) Extracellular matrix degradation and remodeling in development and disease. *Cold Spring Harb. Perspect. Biol.* **3,** a005058
11. Antalis, T. M., Bugge, T. H., and Wu, Q. (2011) Membrane-anchored serine proteases in health and disease. *Prog. Mol. Biol. Transl. Sci.* **99,** 1–50
12. Shi, Y. E., Torri, J., Yieh, L., Wellstein, A., Lippman, M. E., and Dickson, R. B. (1993) Identification and characterization of a novel matrix-degrading protease from hormone-dependent human breast cancer cells. *Cancer Res.* **53,** 1409–1415
13. Benaud, C., Dickson, R. B., and Lin, C. Y. (2001) Regulation of the activity of matriptase on epithelial cell surfaces by a blood-derived factor. *Eur. J. Biochem.* **268,** 1439–1447
14. Lin, C. Y., Anders, J., Johnson, M., Sang, Q. A., and Dickson, R. B. (1999) Molecular cloning of cDNA for matriptase, a matrix-degrading serine protease with trypsin-like activity. *J. Biol. Chem.* **274,** 18231–18236
15. Lin, C. Y., Anders, J., Johnson, M., and Dickson, R. B. (1999) Purification and characterization of a complex containing matriptase and a Kunitz-type serine protease inhibitor from human milk. *J. Biol. Chem.* **274,** 18237–18242

16. Lee, S. L., Dickson, R. B., and Lin, C. Y. (2000) Activation of hepatocyte growth factor and urokinase/plasminogen activator by matriptase, an epithelial membrane serine protease. *J. Biol. Chem.* **275,** 36720–36725
17. Netzel-Arnett, S., Currie, B. M., Szabo, R., Lin, C.-Y., Chen, L.-M., Chai, K. X., Antalis, T. M., Bugge, T. H., and List, K. (2006) Evidence for a matriptase-prostasin proteolytic cascade regulating terminal epidermal differentiation. *J. Biol. Chem.* **281,** 32941–32945
18. Takeuchi, T., Harris, J. L., Huang, W., Yan, K. W., Coughlin, S. R., and Craik, C. S. (2000) Cellular localization of membrane-type serine protease 1 and identification of protease-activated receptor-2 and single-chain urokinase-type plasminogen activator as substrates. *J. Biol. Chem.* **275,** 26333–26342
19. Wu, C.-J., Feng, X., Lu, M., Morimura, S., and Udey, M. C. (2017) Matriptase-mediated cleavage of EpCAM destabilizes claudins and dysregulates intestinal epithelial homeostasis. *J. Clin. Investig.* **127,** 623–634
20. Lai, C.-H., Lai, Y.-J., Chou, F.-P., Chang, H.-H., Tseng, C.-C., Johnson, M. D., Wang, J.-K., and Lin, C.-Y. (2016) Matriptase complexes and prostasin complexes with HAI-1 and HAI-2 in human milk: significant proteolysis in lactation. *PLoS One* **11,** e0152904
21. Szabo, R., Hobson, J. P., Christoph, K., Kosa, P., List, K., and Bugge, T. H. (2009) Regulation of cell surface protease matriptase by HAI2 is essential for placental development, neural tube closure and embryonic survival in mice. *Development* **136,** 2653–2663
22. Fang, J.-D., Chou, H.-C., Tung, H.-H., Huang, P.-Y., and Lee, S.-L. (2011) Endogenous expression of matriptase in neural progenitor cells promotes cell migration and neuron differentiation. *J. Biol. Chem.* **286,** 5667–5679
23. Clark, E. B., Jovov, B., Rooj, A. K., Fuller, C. M., and Benos, D. J. (2010) Proteolytic cleavage of human acid-sensing ion channel 1 by the serine protease matriptase. *J. Biol. Chem.* **285,** 27130–27143
24. Jäckle, F., Schmidt, F., Wichert, R., Arnold, P., Prox, J., Mangold, M., Ohler, A., Pietrzik, C. U., Koudelka, T., Tholey, A., Gütschow, M., Stirnberg, M., and Becker-Pauly, C. (2015) Metalloprotease meprin β is activated by transmembrane serine protease matriptase-2 at the cell surface thereby enhancing APP shedding. *Biochem. J.* **470,** 91–103
25. Beckmann, A.-M., Glebov, K., Walter, J., Merkel, O., Mangold, M., Schmidt, F., Becker-Pauly, C., Gütschow, M., and Stirnberg, M. (2016) The intact Kunitz domain protects the amyloid precursor protein from being processed by matriptase-2. *Biol. Chem.* **397,** 777–790
26. Oberst, M., Anders, J., Xie, B., Singh, B., Ossandon, M., Johnson, M., Dickson, R. B., and Lin, C. Y. (2001) Matriptase and HAI-1 are expressed by normal and malignant epithelial cells *in vitro* and *in vivo*. *Am. J. Pathol.* **158,** 1301–1311
27. Buzza, M. S., Netzel-Arnett, S., Shea-Donohue, T., Zhao, A., Lin, C.-Y., List, K., Szabo, R., Fasano, A., Bugge, T. H., and Antalis, T. M. (2010) Membrane-anchored serine protease matriptase regulates epithelial barrier formation and permeability in the intestine. *Proc. Natl. Acad. Sci. U.S.A.* **107,** 4200–4205
28. Hwang, T., Park, C.-K., Leung, A. K., Gao, Y., Hyde, T. M., Kleinman, J. E., Rajpurohit, A., Tao, R., Shin, J. H., and Weinberger, D. R. (2016) Dynamic regulation of RNA editing in human brain development and disease. *Nat. Neurosci.* **19,** 1093–1099
29. Désilets, A., Béliveau, F., Vandal, G., McDuff, F.-O., Lavigne, P., and Leduc, R. (2008) Mutation G827R in matriptase causing autosomal recessive ichthyosis with hypotrichosis yields an inactive protease. *J. Biol. Chem.* **283,** 10535–10542
30. Lee, M.-S., Tseng, I.-C., Wang, Y., Kiyomiya, K., Johnson, M. D., Dickson, R. B., and Lin, C.-Y. (2007) Autoactivation of matriptase *in vitro*: requirement for biomembrane and LDL receptor domain. *Am. J. Physiol. Cell Physiol.* **293,** C95–C105
31. Brodeur, J., Thériault, C., Lessard-Beaudoin, M., Marcil, A., Dahan, S., and Lavoie, C. (2012) LDLR-related protein 10 (LRP10) regulates amyloid precursor protein (APP) trafficking and processing: evidence for a role in Alzheimer's disease. *Mol. Neurodegener.* **7,** 31
32. Ledesma, M. D., Da Silva, J. S., Crassaerts, K., Delacourte, A., De Strooper, B., and Dotti, C. G. (2000) Brain plasmin enhances APP α-cleavage and Aβ degradation and is reduced in Alzheimer's disease brains. *EMBO Rep.* **1,** 530–535
33. Zhang, Z., Song, M., Liu, X., Su Kang, S., Duong, D. M., Seyfried, N. T., Cao, X., Cheng, L., Sun, Y. E., Ping Yu, S., Jia, J., Levey, A. I., and Ye, K. (2015) δ-Secretase cleaves amyloid precursor protein and regulates the pathogenesis in Alzheimer's disease. *Nat. Commun.* **6,** 8762
34. Toga, A. W., Thompson, P. M., and Sowell, E. R. (2006) Mapping brain maturation. *Trends Neurosci.* **29,** 148–159
35. Paus, T. (2005) Mapping brain maturation and cognitive development during adolescence. *Trends Cogn. Sci.* **9,** 60–68
36. Gogtay, N., Giedd, J. N., Lusk, L., Hayashi, K. M., Greenstein, D., Vaituzis, A. C., Nugent, T. F., 3rd, Herman, D. H., Clasen, L. S., Toga, A. W., Rapoport, J. L., and Thompson, P. M. (2004) Dynamic mapping of human cortical development during childhood through early adulthood. *Proc. Natl. Acad. Sci. U.S.A.* **101,** 8174–8179
37. Kawaguchi, M., and Kataoka, H. (2014) Mechanisms of hepatocyte growth factor activation in cancer tissues. *Cancers* **6,** 1890–1904
38. Uhland, K. (2006) Matriptase and its putative role in cancer. *Cell. Mol. Life Sci.* **63,** 2968–2978
39. List, K., Bugge, T. H., and Szabo, R. (2006) Matriptase: potent proteolysis on the cell surface. *Mol. Med. Camb. Mass.* **12,** 1–7
40. List, K. (2009) Matriptase: a culprit in cancer? *Future Oncol.* **5,** 97–104
41. Miyata, S., Fukushima, T., Kohama, K., Tanaka, H., Takeshima, H., and Kataoka, H. (2007) Roles of Kunitz domains in the anti-invasive effect of hepatocyte growth factor activator inhibitor type 1 in human glioblastoma cells. *Hum. Cell* **20,** 100–106
42. Koivuniemi, R., Mäkelä, J., Hokkanen, M.-E., Bruelle, C., Ho, T. H., Ola, R., Korhonen, L., Schröder, J., Kataoka, H., and Lindholm, D. (2013) Hepatocyte growth factor activator inhibitor-1 is induced by bone morphogenetic proteins and regulates proliferation and cell fate of neural progenitor cells. *PLoS One* **8,** e56117
43. Béliveau, F., Désilets, A., and Leduc, R. (2009) Probing the substrate specificities of matriptase, matriptase-2, hepsin and DESC1 with internally quenched fluorescent peptides. *FEBS J.* **276,** 2213–2226
44. Kirchhofer, D., Peek, M., Li, W., Stamos, J., Eigenbrot, C., Kadkhodayan, S., Elliott, J. M., Corpuz, R. T., Lazarus, R. A., and Moran, P. (2003) Tissue expression, protease specificity, and Kunitz domain functions of hepatocyte growth factor activator inhibitor-1B (HAI-1B), a new splice variant of HAI-1. *J. Biol. Chem.* **278,** 36341–36349
45. Kaden, D., Munter, L. M., Reif, B., and Multhaup, G. (2012) The amyloid precursor protein and its homologues: structural and functional aspects of native and pathogenic oligomerization. *Eur. J. Cell Biol.* **91,** 234–239
46. Hung, R.-J., Hsu, I.-W., Dreiling, J. L., Lee, M.-J., Williams, C. A., Oberst, M. D., Dickson, R. B., and Lin, C.-Y. (2004) Assembly of adherens junctions is required for sphingosine 1-phosphate-induced matriptase accumulation and activation at mammary epithelial cell-cell contacts. *Am. J. Physiol. Cell Physiol.* **286,** C1159–C1169
47. Jin, X., Hirosaki, T., Lin, C.-Y., Dickson, R. B., Higashi, S., Kitamura, H., and Miyazaki, K. (2005) Production of soluble matriptase by human cancer cell lines and cell surface activation of its zymogen by trypsin. *J. Cell. Biochem.* **95,** 632–647
48. O'Brien, R. J., and Wong, P. C. (2011) Amyloid precursor protein processing and Alzheimer's disease. *Annu. Rev. Neurosci.* **34,** 185–204
49. Ludewig, S., and Korte, M. (2016) Novel insights into the physiological function of the APP (gene) family and its proteolytic fragments in synaptic plasticity. *Front. Mol. Neurosci.* **9,** 161
50. Small, D. H., Nurcombe, V., Reed, G., Clarris, H., Moir, R., Beyreuther, K., and Masters, C. L. (1994) A heparin-binding domain in the amyloid protein precursor of Alzheimer's disease is involved in the regulation of neurite outgrowth. *J. Neurosci.* **14,** 2117–2127
51. Nicolas, M., and Hassan, B. A. (2014) Amyloid precursor protein and neural development. *Development* **141,** 2543–2548
52. Willem, M., Tahirovic, S., Busche, M. A., Ovsepian, S. V., Chafai, M., Kootar, S., Hornburg, D., Evans, L. D., Moore, S., Daria, A., Hampel, H., Müller, V., Giudici, C., Nuscher, B., Wenninger-Weinzierl, A., *et al.* (2015) η-Secretase processing of APP inhibits neuronal activity in the hippocampus. *Nature* **526,** 443–447
53. Rossjohn, J., Cappai, R., Feil, S. C., Henry, A., McKinstry, W. J., Galatis, D., Hesse, L., Multhaup, G., Beyreuther, K., Masters, C. L., and Parker, M. W.

(1999) Crystal structure of the N-terminal, growth factor-like domain of Alzheimer amyloid precursor protein. *Nat. Struct. Biol.* **6,** 327–331
54. Kaden, D., Munter, L.-M., Joshi, M., Treiber, C., Weise, C., Bethge, T., Voigt, P., Schaefer, M., Beyermann, M., Reif, B., and Multhaup, G. (2008) Homophilic interactions of the amyloid precursor protein (APP) ectodomain are regulated by the loop region and affect β-secretase cleavage of APP. *J. Biol. Chem.* **283,** 7271–7279
55. Barão, S., Moechars, D., Lichtenthaler, S. F., and De Strooper, B. (2016) BACE1 Physiological functions may limit its use as therapeutic target for Alzheimer's disease. *Trends Neurosci.* **39,** 158–169
56. De Strooper, B. (2014) Lessons from a failed γ-secretase Alzheimer trial. *Cell* **159,** 721–726
57. Désilets, A., Longpré, J.-M., Beaulieu, M.-E., and Leduc, R. (2006) Inhibition of human matriptase by eglin c variants. *FEBS Lett.* **580,** 2227–2232
58. Brosseau, J.-P., Lucier, J.-F., Lapointe, E., Durand, M., Gendron, D., Gervais-Bird, J., Tremblay, K., Perreault, J.-P., and Elela, S. A. (2010) High-throughput quantification of splicing isoforms. *RNA* **16,** 442–449
59. Hellemans, J., Mortier, G., De Paepe, A., Speleman, F., and Vandesompele, J. (2007) qBase relative quantification framework and software for management and automated analysis of real-time quantitative PCR data. *Genome Biol.* **8,** R19
60. Espuny-Camacho, I., Michelsen, K. A., Gall, D., Linaro, D., Hasche, A., Bonnefont, J., Bali, C., Orduz, D., Bilheu, A., Herpoel, A., Lambert, N., Gaspard, N., Péron, S., Schiffmann, S. N., Giugliano, M., *et al.* (2013) Pyramidal neurons derived from human pluripotent stem cells integrate efficiently into mouse brain circuits *in vivo*. *Neuron* **77,** 440–456
61. Gaspard, N., Bouschet, T., Herpoel, A., Naeije, G., van den Ameele, J., and Vanderhaeghen, P. (2009) Generation of cortical neurons from mouse embryonic stem cells. *Nat. Protoc.* **4,** 1454–1463
62. Kim, D., Langmead, B., and Salzberg, S. L. (2015) HISAT: a fast spliced aligner with low memory requirements. *Nat. Methods* **12,** 357–360
63. Liao, Y., Smyth, G. K., and Shi, W. (2014) featureCounts: an efficient general purpose program for assigning sequence reads to genomic features. *Bioinformatics* **30,** 923–930